Int. J. Electron. Commun. (AEÜ) 161 (2023) 154540

Contents lists available at ScienceDirect

International Journal of Electronics and Communications

journal homepage: www.elsevier.com/locate/aeue

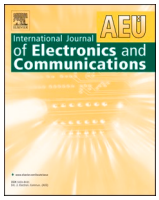

Regular paper

An alternative coupling matrix arrangement for capacitively loaded multi-mode microstrip diplexers having close channel bands

Ceyhun Karpuz [a,*], Pinar Ozturk Ozdemir [b], Hasan Huseyin Balik [c], Adnan Gorur [d]

[a] Department of Electrical and Electronic Engineering, Pamukkale University, Türkiye
[b] Air Force Academy, National Defence University, Türkiye
[c] Faculty of Electrical & Electronics, Computer Engineering, Yildiz Technical University, Türkiye
[d] Department of Electrical and Electronic Engineering, Nigde Omer Halisdemir University, Türkiye

ARTICLE INFO

Keywords:
Microstrip diplexer
Microstrip open loop resonator
Coupling matrix
Loading element
Multi-mode

ABSTRACT

In this paper, a design procedure for multi-mode diplexers having closely located bands and an alternative coupling matrix arrangement suitable for all types are reported. The proposed topology includes the interdigital capacitive fingers as a loading element. In addition, the theoretical approach is based on the combination of a polynomial synthesis procedure and the coupling matrix synthesis method. The validation is shown by the design and fabrication of new microstrip diplexers having two different dual/quad modes bandpass filters to explain how the required selectivity and the isolation between the close channels are obtained. To obtain the best performance without an extra matching circuit, the capacitively loaded loop resonators used as a channel filter are fed by a *T*-junction. To obtain a sufficient coupling effect a serial capacity is used in the input/output. The proposed resonator is investigated by using the even–odd mode analysis to evaluate the resonance frequencies, transmission zeros, and return loss level. An interdigital loading element not only achieves dual-mode characteristics without the requirement of any extra surface area but also moves the transmission zeros to the desired side of the passband. The proposed diplexers have advantages such as compact size, good selectivity, interconnection capability, and high isolation.

1. Introduction

Recently, microwave multiplexers have been widely used in mobile communication and radar systems. The communication systems need diplexers using separated double different signal bands within the wide frequency ranges. The diplexer is one of the fundamental pieces of a transceiver for either splitting a frequency band into two sub-bands or combing two sub-bands into a wide frequency band. Diplexers having a compact size, high isolation, high selectivity, easy fabrication, low cost, etc. are very important for performance of mobile communication systems. Because their performance has very high-density effects on the front-end systems at the radio frequencies (RFs) [1–8]. Modern microwave multiplexer circuits are generally implemented in the planar configurations because of their advantages [9–11]. In [9], a compact diplexer used in the GSM and WLAN applications has been achieved by locating a slotline stepped impedance resonator (SIR) in the ground plane, which performs better out of band rejection and power handling capability. A compact microstrip diplexer consisting of three dual-mode stub-loaded microstrip resonators has been introduced by [10] in which two modes in each of a stub-loaded resonator and one mode in the main resonator are excited to form the lower and higher passbands. The authors have used the *T*-shaped resonator as a frequency selective signal splitter to make the feasible design of a diplexer for a system with two extremely close bands [11]. An approach used in the diplexer design is simply combining two independent filters. The integration of a dual-band filter with additional matching circuits has been reported for reducing the occupied-area of the diplexer circuit [12,13]. However, the extra area of the matching circuit has a disadvantage in reduction of the circuit size. These circuits are not very useful when the TX and the RX bands are extremely close to each other.

In this paper, microstrip diplexers are designed by combining two dual-mode bandpass filters (BPFs) to adjust the center frequencies of the two channels. The design is realized by using a *T*-junction that does not require any combining and matching circuits. Feeding two BPFs from

* Corresponding author.
E-mail addresses: ckarpuz@pau.edu.tr (C. Karpuz), oozdemir33@hho.msu.edu.tr (P. Ozturk Ozdemir), balik@yildiz.edu.tr (H. Huseyin Balik), agorur@ohu.edu.tr (A. Gorur).

https://doi.org/10.1016/j.aeue.2023.154540
Received 11 November 2022; Accepted 12 January 2023
Available online 21 January 2023

the common input port by means of this *T*-junction provides sufficient impedance matching. A theoretical approach is described to exhibit the design procedure for the diplexer. This approach used in the synthesizing of microwave diplexers having very close RX and TX bands is based on the combination of two syntheses proposed in [14,15] for multiport circuits. In [14], a detailed polynomial synthesis procedure is presented for diplexers with arbitrary topology while the coupling matrix synthesis having analytical and exact method properties is described for the three-port circuits in [15]. The proposed synthesis procedure starts to determine suitable reflection and transmission zeros or poles for a desired symmetrical frequency response of RX/TX channel filters then a polynomial synthesis is realized for Hurwitz factorization to obtain the relationships between the admittance parameters and scattering parameters of the three-port circuit. Finally, the coupling matrix elements involved residues of the admittance parameters and source-load coupling of each output are calculated by means of these relationships.

One of the main goals of diplexer designs is to achieve good isolation between the output ports. To improve the diplexer isolation, the location of the transmission zero (TZ) for a channel filter has been arranged as to be at the passband of the other channel filter. As is well known in the literature [16], the dual-mode characteristic for conventional loop filters is obtained by excitation of degenerate modes with a perturbation element which this excitation provides a pair of TZs whereas a loading element is used for open loop resonators [17], in this case, a single TZ occurs near the passband. The location of the TZ can simply be determined depending on the configuration of the loading element. The moving of the transmission zeros from the left/right side of the passband to the right/left side is a very important factor to achieve the reconfigurable filtering characteristics, which is quite important to provide sufficient isolation and desired selectivity. Therefore, these open loop resonators are used to design a diplexer with high selectivity and good isolation between the channel bands, in this paper. The proposed diplexers have been simulated and fabricated and tested to validate the theoretical and simulated results.

The organization of this paper is arranged as follows. In Section 2, the theoretical approach for the three-port circuit topology is described based on the combination of a polynomial synthesis procedure and the coupling matrix synthesis method. Section 3.1 reports an analysis of the capacitively loaded dual-mode resonator. The frequency responses obtained from the configuration of the loading element and the arrangement of the open loop resonator are also investigated in this section. As is shown in Sections 3.2 and 3.3, the diplexer circuits having some properties such as dual-mode, quad-mode and controllable transmission zeros providing an effective selectivity can easily be constructed by using the capacitively loaded and coupled resonators. Finally, Section 4 includes the performance test of the experimental studies to demonstrate the validity of the proposed diplexer design.

2. Modification of coupling matrix technique for multi-mode diplexers

In the design, a *T*-junction is used to combine two channel filters having different sizes to avoid using an additional matching circuit. The *T*-junction used in the input port of the diplexer behaves as an impedance matching circuit, which is important to reduce the circuit size. Thus, it is no need to use any extra matching circuit. Fig. 1(A) depicts the general architecture of a diplexer, which is formed by extremely close RX and TX bands with BPF topology. The proposed synthesis procedure of the diplexer starts with determining suitable reflection and transmission zeros or poles for a desired symmetrical frequency response of RX/TX channel filters. Then a polynomial synthesis is realized for Hurwitz factorization to obtain the relationships between the admittance parameters and scattering parameters of the three-port circuit. Finally, the coupling matrix elements involved residues of the admittance parameters, and the source-load coupling of each output is calculated by means of these relationships. Thus, the frequency response

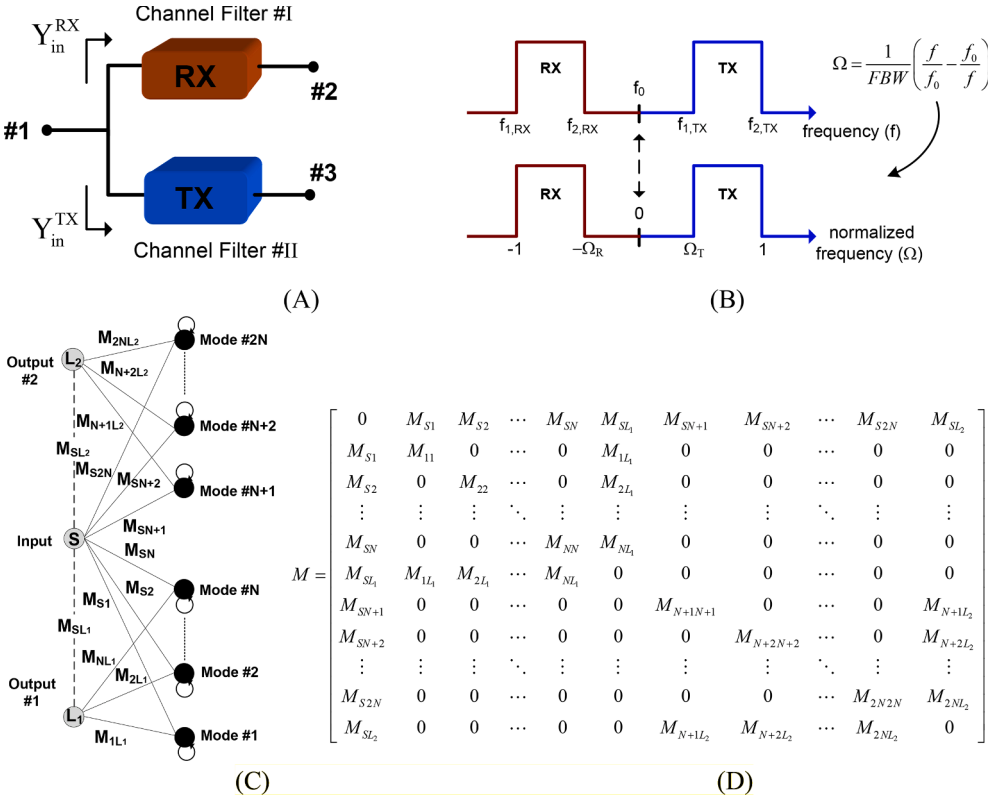

Fig. 1. (A) Architecture of general diplexer without using any impedance matching circuit (B) the frequency transform diagram (C) coupling diagram and (D) proposed general coupling matrix for a diplexer with transversal form.

of the whole diplexer instead of each filter is obtained from the admittance parameters.

The first step for synthesis of the diplexer is to describe the normalized frequencies, which the related frequency points are shown in Fig. 1(B). The synthesis procedure given in [14] occurs by deriving polynomials with a specific junction topology. Four polynomials are required to define the S parameters of the proposed diplexer circuit since it is a three-port circuit as formulated in (1). These polynomials are obtained by using reflection zeros at the input port of the diplexer and transmission zeros of the channel filters, as indicated in [14].

$$S_{11}(s)=\frac{F(s)}{E(s)},\ S_{21}(s)=\frac{P_r(s)}{E(s)},\ S_{31}(s)=\frac{P_t(s)}{E(s)} \tag{1}$$

where *E(s)* is the common denominator polynomial of the reflection and transfer functions while *F(s)* represents the numerator polynomial of the reflection function. Also, $P_r(s)$ and $P_t(s)$ are the numerator polynomials of the transfer function for RX and TX channel filters, respectively, which their roots denote the transmission zeros for output ports while the roots of *F(s)* are the reflection zeros for the input port of the diplexer. They are necessary to calculate the input admittance to derive the characteristic polynomials of the diplexer by considering the expressions of the scattering parameters given in (2).

$$\begin{aligned} S_{11}&=\frac{1-Y_{in}}{1+Y_{in}},\\ S_{21}&=\frac{S_{21}^{RX}\left(1+Y_{in}^{RX}\right)}{1+Y_{in}^{RX}+Y_{in}^{TX}},\\ S_{31}&=\frac{S_{21}^{TX}\left(1+Y_{in}^{TX}\right)}{1+Y_{in}^{RX}+Y_{in}^{TX}} \end{aligned} \tag{2}$$

The input admittance at common port 1 (Y_{in}) is calculated as the sum of the input admittances of the two channel filters (Y_{in}^{RX},Y_{in}^{TX}), as can be seen in Fig. 1(A). Characteristic polynomials of the channel filters primarily need to be obtained independently from the diplexer to obtain the polynomials given in (2). At this stage, the characteristic polynomials of RX and TX filters are defined in (3) and (4), respectively. The polynomials are calculated using the methods available in [18].

$$S_{11}^{RX}(s)=\frac{F_{RX}(s)}{E_{RX}(s)},\ S_{21}^{RX}(s)=\frac{p_0^{RX}\ P_{RX}(s)}{E_{RX}(s)} \tag{3}$$

$$S_{11}^{TX}(s)=\frac{F_{TX}(s)}{E_{TX}(s)},\ S_{21}^{TX}(s)=\frac{p_0^{TX}\ P_{TX}(s)}{E_{TX}(s)} \tag{4}$$

where $E_{RX/TX}(s)$ are common denominator polynomials of the reflection and transfer functions for RX and TX filters, respectively. The roots of $F_{RX/TX}(s)$ represent the reflection zeros while the roots of $P_{RX/TX}(s)$ indicate the transmission zeros. The highest degrees of $P_{RX/TX}(s)$ are equal to 1 because of normalized polynomials with their suitable coefficients (p_0^{RX}/p_0^{TX}). The relationship between the transmission polynomials of channel filters and the diplexer can be explained by (5) and (6).

$$P_r(s)=p_0^{RX}P_{RX}(s)\frac{E_{TX}(s)+F_{TX}(s)}{2} \tag{5}$$

$$P_t(s)=p_0^{TX}P_{TX}(s)\frac{E_{RX}(s)+F_{RX}(s)}{2} \tag{6}$$

To obtain the coupling matrix of the proposed diplexer, after obtaining these characteristic polynomials, the next step in the theoretical approach is to develop the methods used in the literature [19,20]. Following to derive of the diplexer polynomials using the set of formulas in (1)–(6), the synthesis of the rational functions that give the admittance parameters (y_{11}, y_{21}, and y_{31}) can be described. These parameters are necessary for achieving the coupling matrix of the diplexer circuit. The matrix of admittance parameters can be calculated from the scattering parameters by the matrix equation, as shown in (7).

$$[Y]=[Z_0]^{-1}([U]-[S])([U]-[S])^{-1}[Z_0]^{-1} \tag{7}$$

$[Z_0]$ is the diagonal matrix of reference impedances at each port of the circuit, [U] is the identity matrix, and [S] is the scattering matrix [15]. The rational polynomials of the short-circuit admittance parameters (y_{11}, y_{21}, y_{31}) can be calculated based on the method prescribed in [20]. It should be noted that the admittance parameters must be arranged by using the rational characteristic polynomials given in (1) according to the three-port circuit. As is well known [14] that the denominator polynomials are equal to each other so that$y_{11d}(s)=y_{21d}(s)=y_{31d}(s)=y_d(s)$. Thus;

$$\begin{aligned} y_{11}(s)&=\frac{y_{11n}(s)}{y_d(s)}=\frac{n_1(s)}{m_1(s)},\\ y_{21}(s)&=\frac{y_{21n}(s)}{y_d(s)}=\frac{P_r(s)}{m_1(s)},\\ y_{31}(s)&=\frac{y_{31n}(s)}{y_d(s)}=\frac{P_t(s)}{m_1(s)} \end{aligned} \tag{8}$$

where

$$m_1(s)=Re(e_0+f_0)+jIm(e_1+f_1)+Re(e_2+f_2)+\ldots \tag{9}$$

$$n_1(s)=jIm(e_0+f_0)+Re(e_1+f_1)+jIm(e_2+f_2)+\ldots \tag{10}$$

e_i and f_i i = 0,1, 2, …, 2 N (N is the degree of each identical channel filter) are the complex coefficient of the E(s) and F(s) polynomials of the diplexer circuit, and the degree of these polynomials is the same in case the degree of the denominator is less than that of the numerator for all channel filter types. The degree of $P_r(s)$ and $P_t(s)$ is equal to the crossways sum of reflection and transmission zero numbers for RX and TX, respectively. As mentioned above, to obtain the admittance parameters $y_{11}(s)$, $y_{21}(s)$, and $y_{31}(s)$ in (8), the realizing of the rational polynomials synthesis including the Hurwitz factorization procedure provides to determine E(s), F(s), $P_r(s)$, and $P_t(s)$ polynomials. In this case, the admittance matrix for the proposed diplexer becomes

$$\begin{bmatrix} y_{11}(s) & y_{12}(s) & y_{13}(s)\\ y_{21}(s) & y_{22}(s) & y_{23}(s)\\ y_{31}(s) & y_{32}(s) & y_{33}(s) \end{bmatrix}=j\begin{bmatrix} 0 & K_0^{RX} & K_0^{TX}\\ K_0^{RX} & 0 & 0\\ K_0^{TX} & 0 & 0 \end{bmatrix}+\sum_{k=1}^{N}\frac{1}{(s-j\lambda_k)}\begin{bmatrix} r_{11k} & r_{12k} & r_{13k}\\ r_{21k} & r_{22k} & r_{23k}\\ r_{31k} & r_{32k} & r_{33k} \end{bmatrix} \tag{11}$$

where $K_0^{RX/TX}$ are couplings between the input and RX/TX outputs (source-load couplings) that are non-zero when the number of transmission zeros is equal to the filtering degree similar to the definition in [20]. λ_k real eigenvalues (k = 1, 2, 3, …, N) are the roots of the common denominator polynomial ($m_1(s)$) of the admittance parameters. r_{ijk} (i, j = 1,2,3 and k = 1, 2, 3, …, N) are residues of the numerator and denominator polynomials for $y_{11}(s)$, $y_{21}(s)$, and $y_{31}(s)$ at λ_k eigenvalues and can easily be obtained by using the residue calculation techniques in the complex analysis. It is noted that these residues are the coefficients in the case of the partial fraction expansions for the admittance parameters and are also related to not only the self-coupling of the modes but also between input/outputs and modes.

The source-load couplings are calculated from

$$K_0^{RX}=-j\frac{y_{21n}(s)}{y_d(s)}\bigg|_{s=j\infty} \tag{12a}$$

$$K_0^{TX}=-j\frac{y_{31n}(s)}{y_d(s)}\bigg|_{s=j\infty} \tag{12b}$$

where $y_d(s)$ is the common denominator polynomial while $y_{21n}(s)$ and $y_{31n}(s)$ are the numerator polynomials. Coupling matrices of the coupling diagram proposed for transversal formed diplexers shown in

Fig. 1(C) are named initial coupling matrices. A general form for these matrices is given in Fig. 1(D) and the values of coupling elements are calculated by using the following equations.

$$\begin{bmatrix} y_{11}(s) & y_{12}(s) & y_{13}(s) \\ y_{21}(s) & y_{22}(s) & y_{23}(s) \\ y_{31}(s) & y_{32}(s) & y_{33}(s) \end{bmatrix} = \left[Y_{SL_1/SL_2}\right] + \sum_{k=1}^{N} \begin{bmatrix} Y_{11k} & Y_{12k} & Y_{13k} \\ Y_{21k} & Y_{22k} & Y_{23k} \\ Y_{31k} & Y_{32k} & Y_{33k} \end{bmatrix}$$

$$= j \begin{bmatrix} 0 & M_{SL_1} & M_{SL_2} \\ M_{SL_1} & 0 & 0 \\ M_{SL_2} & 0 & 0 \end{bmatrix} + \sum_{k=1}^{N} \frac{1}{(s - j\lambda_k)} \begin{bmatrix} M_{Sk}^2 & M_{Sk}M_{kL_1} & M_{Sk}M_{kL_2} \\ M_{Sk}M_{kL_1} & M_{kL_1}^2 & M_{kL_1}M_{kL_2} \\ M_{Sk}M_{kL_2} & M_{kL_1}M_{kL_2} & M_{kL_2}^2 \end{bmatrix} \tag{13}$$

As mentioned above, the coupling matrix elements ($M_{i,j}$) in Fig. 1(D) are related to the elements values of the admittance matrix in (13), which can easily be calculated r_{ijk} residues in (11) by using the following equations.

$$M_{Sk} = \sqrt{r_{11k}} \tag{14}$$

$$M_{kL_1} = \frac{r_{21k}}{\sqrt{r_{11k}}} \tag{15}$$

$$M_{kL_2} = \frac{r_{31k}}{\sqrt{r_{11k}}} \tag{16}$$

$$M_{kk} = \lambda_k,\ k = 1,\ 2,\ 3,\ \ldots,\ 2N \tag{17}$$

These equations can be used to calculate all the non-zero elements of the coupling matrix by its admittance parameters for the coupling diagram corresponding to the diplexer topology.

The general equation may be expressed as follows to derive the S-parameters for the three-port circuit.

$$S_{11} = 1 - \frac{2}{q_{e,0}}[\mathrm{A}]^{-1}_{0,0} \tag{18}$$

$$S_{21} = \frac{2}{\sqrt{q_{e,0}q_{e,(N+1)}}}[\mathrm{A}]^{-1}_{(N+1),0},\ S_{31} = \frac{2}{\sqrt{q_{e,0}q_{e,(2N+2)}}}[\mathrm{A}]^{-1}_{(2N+2),0} \tag{19}$$

by using

$$[\mathrm{A}] = [q] + p[U] - j[M] \tag{20}$$

where p is the complex frequency variable, [M] is the coupling matrix, [U] is the identity matrix, [q] is zero matrix, except for $q_{0,0} = 1/q_{e,0}$,$q_{(N+1),0} = 1/q_{e,(N+1)}$, and$q_{(2N+2),0} = 1/q_{e,(2N+2)}$. All matrices are $(2N+3) \times (2N+3)$ reciprocal matrices ($M_{i,j} = M_{j,i}$).

The approach method explained in detail above is an effective and suitable method for synthesizing microwave diplexers having symmetric or asymmetric characteristics. To illustrate the proposed synthesis procedure, a diplexer constructed with two dual-mode channel filters having a symmetric frequency response with a pair of transmission zeros has been synthesized as a sample three-port circuit. Sample coupling diagrams for transversal and folded form dual-mode diplexers are shown in Fig. 2(A) and 2(C) while their coupling matrices are depicted in Fig. 2 (B) and 2(D), respectively. As is well known, the coupling matrix of transversal form is called "initial coupling matrix form", which is obtained from (14)-(17). Then, to obtain the proposed coupling matrix shown in Fig. 2(D), similarity transformations can be applied to this initial coupling matrix [20].

Firstly, specifications for the channel filters are determined to use in the applying example of the proposed diplexer synthesis. RX/TX channel filters have dual-mode characteristics and passbands with − 20 dB return loss at center frequencies. The transmission zeros are located at − 9.45 and 1.45 for RX, −1.45 and 9.45 for TX. The reflection zeros placed at − j4.27, −j3.72 for RX, j3.72 and j4.27 for TX, have a symmetrical distribution according to the center frequencies of the channel filters. Also, the rejection level of the out-of-band is better than − 30 dB for each filter.

For these specifications, the synthesis procedure steps are briefly explained as follows:

- Specifying the channel filter properties such as center frequency, bandwidth, selectivity, return loss or insertion loss level, etc.
- Computing the characteristic polynomials of channel filters given in (3)–(4) by using the quasi-elliptical filtering characteristic [18] based on the prescribed RX/TX specifications.
- Acquiring the diplexer's reflection and transfer functions by employing characteristic RX and TX polynomials with formulas in (1)–(2) and (5)–(6). (seen in Table 1.).

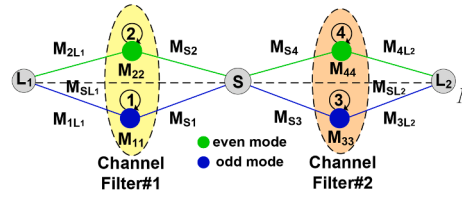

(A)

$$M = \begin{array}{c|cccccccc} & \mathbf{S} & \mathbf{1} & \mathbf{2} & \mathbf{L_1} & \mathbf{3} & \mathbf{4} & \mathbf{L_2} \\ \mathbf{S} & 0 & M_{S1} & M_{S2} & M_{SL_1} & M_{S3} & M_{S4} & M_{SL_2} \\ \mathbf{1} & M_{S1} & M_{11} & 0 & M_{1L_1} & 0 & 0 & 0 \\ \mathbf{2} & M_{S2} & 0 & M_{22} & M_{2L_1} & 0 & 0 & 0 \\ \mathbf{L_1} & M_{SL_1} & M_{1L_1} & M_{2L_1} & 0 & 0 & 0 & 0 \\ \mathbf{3} & M_{S3} & 0 & 0 & 0 & M_{33} & 0 & M_{3L_2} \\ \mathbf{4} & M_{S4} & 0 & 0 & 0 & 0 & M_{44} & M_{4L_2} \\ \mathbf{L_2} & M_{SL_2} & 0 & 0 & 0 & M_{3L_2} & M_{4L_2} & 0 \end{array}$$

(B)

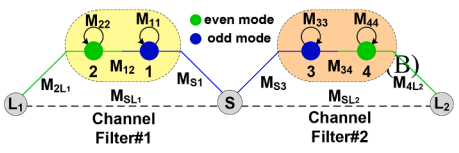

(C)

$$M = \begin{array}{c|cccccccc} & \mathbf{S} & \mathbf{1} & \mathbf{2} & \mathbf{L_1} & \mathbf{3} & \mathbf{4} & \mathbf{L_2} \\ \mathbf{S} & 0 & M_{S1} & 0 & M_{SL_1} & M_{S3} & 0 & M_{SL_2} \\ \mathbf{1} & M_{S1} & M_{11} & M_{12} & 0 & 0 & 0 & 0 \\ \mathbf{2} & 0 & M_{12} & M_{22} & M_{2L_1} & 0 & 0 & 0 \\ \mathbf{L_1} & M_{SL_1} & 0 & M_{2L_1} & 0 & 0 & 0 & 0 \\ \mathbf{3} & M_{S3} & 0 & 0 & 0 & M_{33} & M_{34} & 0 \\ \mathbf{4} & 0 & 0 & 0 & 0 & M_{34} & M_{44} & M_{4L_2} \\ \mathbf{L_2} & M_{SL_2} & 0 & 0 & 0 & 0 & M_{4L_2} & 0 \end{array}$$

(D)

Fig. 2. Coupling diagrams and coupling matrices for different configurations of dual-mode diplexers; (A) and (B) for transversal, (C) and (D) folded forms, respectively.

- Calculating numerator and denominator polynomials of the admittance parameters by using rational characteristic polynomials (given in (8)–(10)).
- After synthesizing procedure, deriving the coupling matrix from the reflection and transfer functions of the diplexer by means of (11)–(13).
- Computing the residues of y11(s), y21(s), and y31(s) to find values of the initial coupling matrix elements (seen in (14)–(17)).
- Obtaining S-parameters of the three-port circuit by using the formulas in (18)–(20).

The coefficients of rational characteristic polynomials normalized according to the highest coefficient of E(s) are given in Table 1 for the dual-mode diplexer.

After applying the synthesis process steps, the elements of the proposed coupling matrix corresponding to the transversal coupling diagram in Fig. 2(A) are obtained as

$$\begin{bmatrix} & \mathbf{S} & \mathbf{1} & \mathbf{2} & \mathbf{L_1} & \mathbf{3} & \mathbf{4} & \mathbf{L_2} \\ \mathbf{S} & 0 & 0.542 & 0.525 & -0.012 & 0.525 & 0.542 & -0.012 \\ \mathbf{1} & 0.542 & -4.658 & 0 & -0.524 & 0 & 0 & 0 \\ \mathbf{2} & 0.525 & 0 & -3.383 & 0.541 & 0 & 0 & 0 \\ \mathbf{L_1} & -0.012 & -0.524 & 0.541 & 0 & 0 & 0 & 0 \\ \mathbf{3} & 0.525 & 0 & 0 & 0 & 0.383 & 0 & -0.541 \\ \mathbf{4} & 0.542 & 0 & 0 & 0 & 0 & 4.658 & 0.524 \\ \mathbf{L_2} & -0.012 & 0 & 0 & 0 & -0.541 & 0.524 & 0 \end{bmatrix} \quad (21)$$

where S and, L_1/L_2 represents the input port and output ports, respectively. Coupling elements in the first row/column of the coupling matrix represent the coupling between the common input port, output ports and modes of the channel filters. Nodes 1–2 and 3–4 depict modes of channel filters #1 and #2, respectively. All non-zero element in the matrix corresponds to a physical coupling element in the diplexer topology. Diagonal elements in the matrix, M_{ii} represents the self-coupling of the modes and M_{ij} ($i \neq j$) shows the coupling between the modes. The frequency response calculated by using this coupling matrix is shown in Fig. 3.

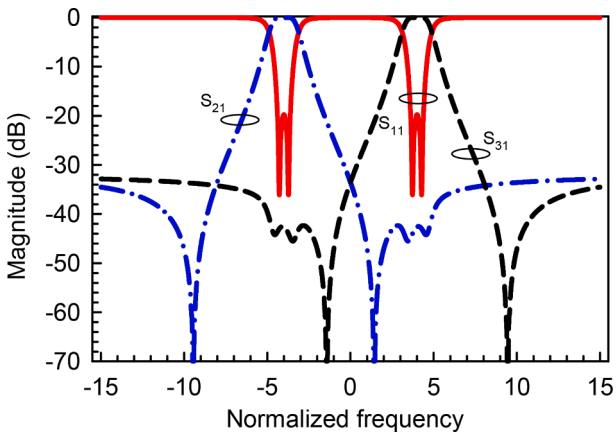

Fig. 3. Calculated frequency response for both transversal and folded forms having two-channel filters with the symmetric dual-mode characteristic.

Alternatively, the coupling diagrams for the transversal and folded form quad-mode diplexers are given in Fig. 4(A) and 4(C), respectively. For synthesizing such a quad-mode diplexer configuration, the fourth-order RX having transmission zeros at − 16.75, −9.45, 1.45, and 8.75, and TX having transmission zeros at − 8.75, −1.45, 9.45, and 16.75 are considered. The reflection zeros of RX/TX are located at ± j2.27, ±j3.26, ±j4.73and ± j5.72 in their passbands. Each filter has return loss of − 25 dB at their center frequencies. The rejection level of out-of-band is better than − 40 dB for RX/TX. The coupling matrix of the quad-mode diplexer can be calculated by following the synthesis procedure steps given for the dual-mode diplexer above. In this case, the resulting polynomials of the quad-mode diplexer are seen in Table 2.

After determining these polynomials, the synthesis procedure yields the initial coupling matrix in Fig. 4(B). Then, to obtain the proposed coupling matrix in Fig. 4(D), similarity transformations described in [20] can be applied to the initial coupling matrix. As a result, the values of the coupling matrix elements are found as

$$\begin{bmatrix} & \mathbf{S} & \mathbf{1} & \mathbf{2} & \mathbf{3} & \mathbf{4} & \mathbf{L_1} & \mathbf{5} & \mathbf{6} & \mathbf{7} & \mathbf{8} & \mathbf{L_2} \\ \mathbf{S} & 0 & 0.871 & 1.292 & 0 & 0 & -0.003 & 0.871 & 1.292 & 0 & 0 & -0.003 \\ \mathbf{1} & 0.871 & -5.508 & 0 & 0 & -2.317 & 0 & 0 & 0 & 0 & 0 & 0 \\ \mathbf{2} & 1.292 & 0 & -4.351 & 1.388 & 0 & 0 & 0 & 0 & 0 & 0 & 0 \\ \mathbf{3} & 0 & 0 & 1.388 & -4.182 & 0 & 1.334 & 0 & 0 & 0 & 0 & 0 \\ \mathbf{4} & 0 & -2.317 & 0 & 0 & -2.715 & 0.949 & 0 & 0 & 0 & 0 & 0 \\ \mathbf{L_1} & -0.003 & 0 & 0 & 1.334 & 0.949 & 0 & 0 & 0 & 0 & 0 & 0 \\ \mathbf{5} & 0.871 & 0 & 0 & 0 & 0 & 0 & 5.508 & 0 & 0 & 2.317 & 0 \\ \mathbf{6} & 1.292 & 0 & 0 & 0 & 0 & 0 & 0 & 4.351 & -1.388 & 0 & 0 \\ \mathbf{7} & 0 & 0 & 0 & 0 & 0 & 0 & 0 & -1.388 & 4.182 & 0 & -1.334 \\ \mathbf{8} & 0 & 0 & 0 & 0 & 0 & 0 & 2.317 & 0 & 0 & 2.715 & -0.949 \\ \mathbf{L_2} & -0.003 & 0 & 0 & 0 & 0 & 0 & 0 & 0 & -1.334 & -0.949 & 0 \end{bmatrix} \quad (22)$$

Table 1
The coefficients of the rational characteristic polynomials for dual-mode diplexer.

Coefficient (c_n)	Rational Characteristic Polynomials $\sum_{n=0}^{4} c_n s^n = c_4 s^4 + c_3 s^3 + c_2 s^2 + c_1 s^1 + c_0$			
	$E(s)$	$F(s)$	$P_r(s)$	$P_t(s)$
c_4	1	0.999	0.0249	0.0249
c_3	2.279	− 0.000176	0.0142	0.0142
c_2	34.459	31.804	1.544 + 0.057i	1.544–0.057i
c_1	37.788	− 0.384	0.648 − 5.8231i	0.648 + 5.8231i
c_0	248.281	248.164	−5.312–0.777i	−5.312 + 0.777i

where nodes 1–4 and 5–8 represent modes of channel filters #1 and #2, as depicted in the folded coupling diagram (see Fig. 4(C)). Diagonal elements in the matrix, M_{ii} represents the self-coupling of the modes and M_{ij} ($i \neq j$) shows the coupling between the modes. The response of the coupling matrix is seen in Fig. 5, where it is clear that it meets all the prescribed specifications.

3. Design steps for proposed multi-mode diplexer

In this section, the microstrip diplexers with a *T*-junction are employed to demonstrate the validation of the theoretical approach. This paper focuses on diplexer applications without using any

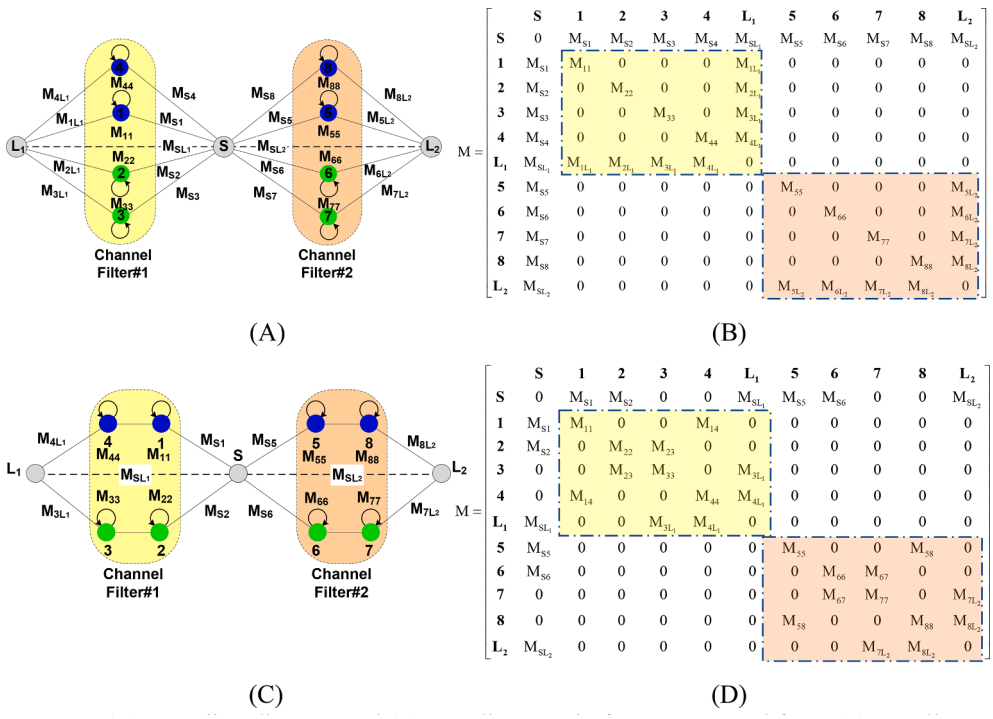

Fig. 4. (A) Coupling diagram and (B) coupling matrix for a transversal form (C) coupling diagram and (D) coupling matrix for a folded form of quad-mode diplexer configuration.

Table 2
The coefficients of the rational characteristic polynomials for quad-mode diplexer having symmetrical frequency response.

Coefficients (c_n)	Rational Characteristic Polynomials $\sum_{n=0}^{8} c_n s^n = c_8 s^8 + c_7 s^7 + c_6 s^6 + c_5 s^5 + c_4 s^4 + c_3 s^3 + c_2 s^2 + c_1 s^1 + c_0$			
	$E(s)$	$F(s)$	$P_r(s)$	$P_t(s)$
c_8	1	0.999	0.005897	0.005897
c_7	9.717	− 0.0000422	0.0143	0.0143
c_6	112.333	65.104	1.566 + 0.057i	1.566 − 0.057i
c_5	643.039	−28.693	3.525 − 8.627i	3.525 + 8.627i
c_4	3338.417	1276.792	67.317 − 7.268i	67.317 + 7.268i
c_3	10409.22	− 1150.288	181.664 − 730.212i	181.664 + 730.212i
c_2	24366.66	8679.012	− 2323.51 − 1063.94i	− 2323.51 + 1063.94i
c_1	29410.8	− 7254.708	− 1962.21 + 3051.54i	− 1962.21 − 3051.54i
c_0	24393.42	24253.16	1427.27 + 1172.35i	1427.27 − 1172.35i

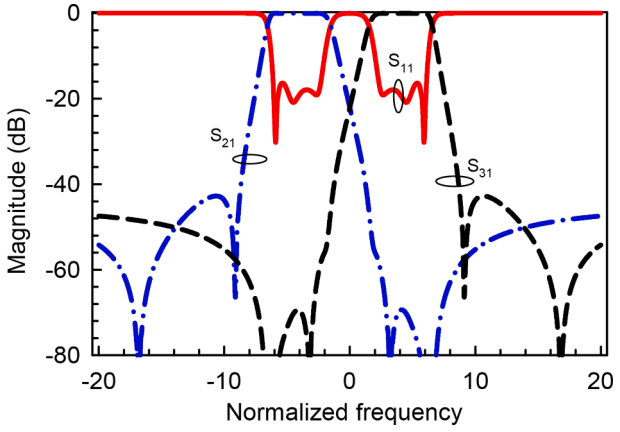

Fig. 5. Calculated frequency response for both transversal and folded forms of the diplexer with two-channel filters having symmetric fourth-degree characteristics.

impedance matching circuit. The diplexer circuit based on a dual-mode open loop resonator with a loading element can provide extremely close frequency bands. The advantage of using such a resonator is that it provides the possibility to be located a transmission zero on any side of the passband. Utilization of the coupled open loop resonator with a loading element increases the channel order and results in a compact circuit size. The designed diplexers are based on the combination of two filters, and the filters are arranged using the *T*-junction to acquire a convenient configuration. Two microstrip diplexer designs are presented in this section. The first one is a diplexer having two dual-mode channel filters with asymmetric frequency response. The other has two asymmetric channel filters with quad-mode and transmission zeros on both sides of the passband. The dimensions of the resonators can be determined based on the resonator analysis to adjust the desired center frequencies of the channel filters in all designed circuits. In addition, parameters of the loading element can be determined by using this analysis to achieve multi-mode in the passband.

The design processes can be briefly summarized in 5 steps.

Step 1- Specifying the channel filter properties such as center frequency, bandwidth, selectivity, return loss or insertion loss level, etc.
Step 2- Determining for each channel separately the dimension of the open loop resonators by means of the even–odd mode analysis based on the filter specification in Step 1.
Step 3- Adjusting the location of the transmission zeros as regards the value of the loading element parameters (l_1, l_2) and the tap point position (t) based on a desired external quality factor.
Step 4- Constructing the dual-mode diplexer by using the channel filters (RX/TX) operating at lower and higher frequencies.

Step 5- Constructing the quad mode diplexer based on the multi-mode obtained by using the coupling gap arrangement of the capacitively-loaded resonators in each passband.

For Step 4, a single TZ occurs on the left/right side of the passband according to the even mode frequency lower/higher than that of the odd mode as relating to the value of the loading element parameters (l_1, l_2). Thus, dual-mode diplexer is designed by connecting the two bandpass channel filters having different electrical lengths with a *T*-junction to achieve the required input matching at the two channels of the diplexer.

For Step 5, three TZs occur on the left/right side of the passband. While one of them (called natural TZ) is a result of the coupling between two resonators, the others are related to the coupling between the even mode of the resonators. The left/right side location of them are arranged by changing the even mode frequency as explained in Step 4. As a result, increasing or decreasing of channel filter selectivity of the diplexer in case of the presence or absence of the TZs located on the left/right side of the passband provides design flexibility that is a very important factor for designers. While the quad mode is obtained by coupling the two identical dual-mode resonators, the quad mode diplexer is designed by connecting the two quad mode bandpass channel filters the same way as in the previous step.

Detailed design concepts are given in the following subsections.

3.1. Dual-mode resonator design

Two different center frequencies should be specified to realize the left and right passband filters. As can be seen in the flowchart given in Fig. 6(A), the first step of the design is determining the electrical length of the open loop resonators according to the center frequencies of the filters. At the same time, miniaturization is achieved in dimensions by obtaining dual-mode with a single resonator utilizing a loading element. Since the open loop resonator with a loading element excites two modes, the dual-mode microstrip open loop resonators for the design of the channel filters are firstly investigated in this section. The two degenerate modes are split by virtue of a loading element, as discussed in [17]. However, the effect of the patch loading element is limited since the loading element will be placed into the resonator shown in Fig. 7(A). This limitation can be annihilated by the slow-wave effect constructed by means of the loading element. It can be seen from Fig. 7(B) that the loading element is occurred by an interdigital structure composed of the combination of the interdigital unit cells. The interdigital unit cells placed as the loading element ensure that the structure becomes more capacitive. Additionally, the interdigital structure is connected to the resonator by means of an inductive line. The capacitance and inductance per unit length of the loading element can be adjusted by the lengths of the interdigital fingers and the inductive line (l_1, l_2), respectively. Configuration of the loading element can be varied geometrically according to the required capacitive or inductive effect. An equivalent circuit of the single/dual-mode open loop resonator is shown in Fig. 7 (C). C_s is the total serial capacitance by representing the required coupling strength between the input/output feed lines and the resonator. It is noted that C_s includes the lumped capacitor (C_f) used to adjust the energy level required in case the connection of the loading elements to the open loop resonators for obtaining the dual-mode characteristic. The electrical length of the resonator is equal to $2(\theta_1 + \theta_2)$, which is equivalent to $\lambda/2$ at the resonance frequency. The electrical lengths of the transmission lines (θ_1 and θ_2 for the top and bottom arms of the resonator, respectively) are based on the tap point (t). The values of t can be adjusted by changing the connection point of the lumped capacitor (C_f). The gap of the microstrip open loop resonator is represented by a π-equivalent circuit model, as depicted in Fig. 7(C). While the loading element is not used for the single-mode, an interdigital loading element is connected to the open loop resonator to obtain the dual-mode characteristic. The interdigital structure is connected to the ground by vias on one side to occur the shunt capacitance effect. The change of the fundamental parameters such as the number of unit cells, the width and length of the finger, and the space between the fingers determine the capacitance the width and length of the finger, and the space between the fingers determine the capacitance per unit length of the structure. At the same time, this structure is connected to the resonator by a thin inductive line at the middle point of the bottom arm of the resonator. Therefore, the loading element can represent by a variable capacitor and inductor connected in series due to its geometrical variation. Meanwhile, the interdigital unit cells result in compact circuit size.

It should be noted that since the widths of the top and bottom arms are equal, their characteristic admittances in the equivalent circuit model are also equal ($Y_{01} = Y_{02}$). For even–odd mode analysis, the

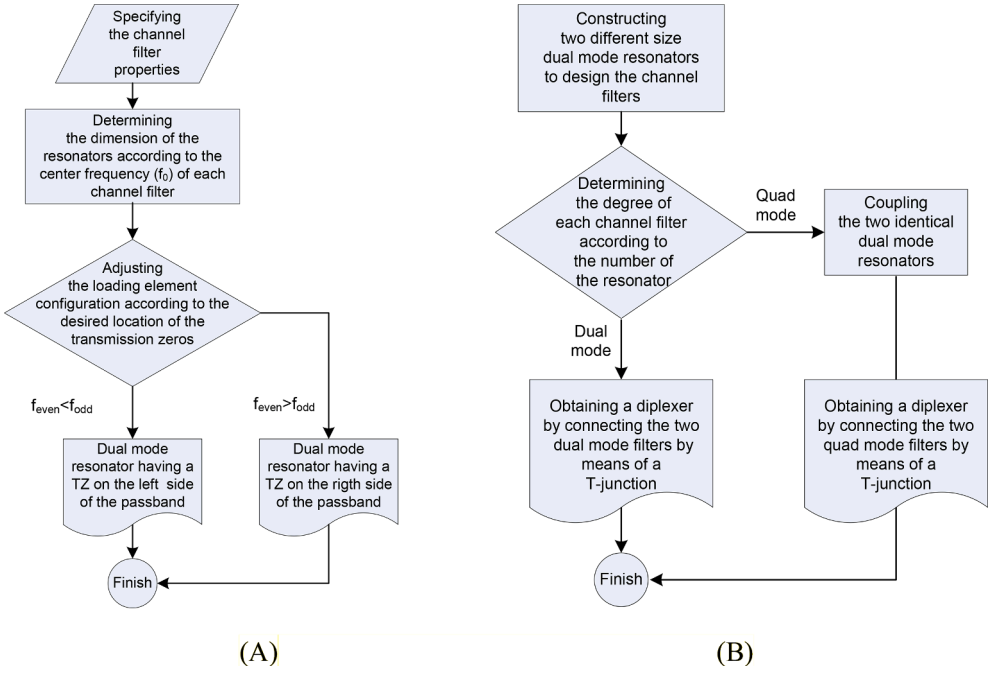

Fig. 6. Design steps of the (A) constructing the dual-mode open loop resonator having a transmission zero (B) the dual/quad mode diplexer circuit.

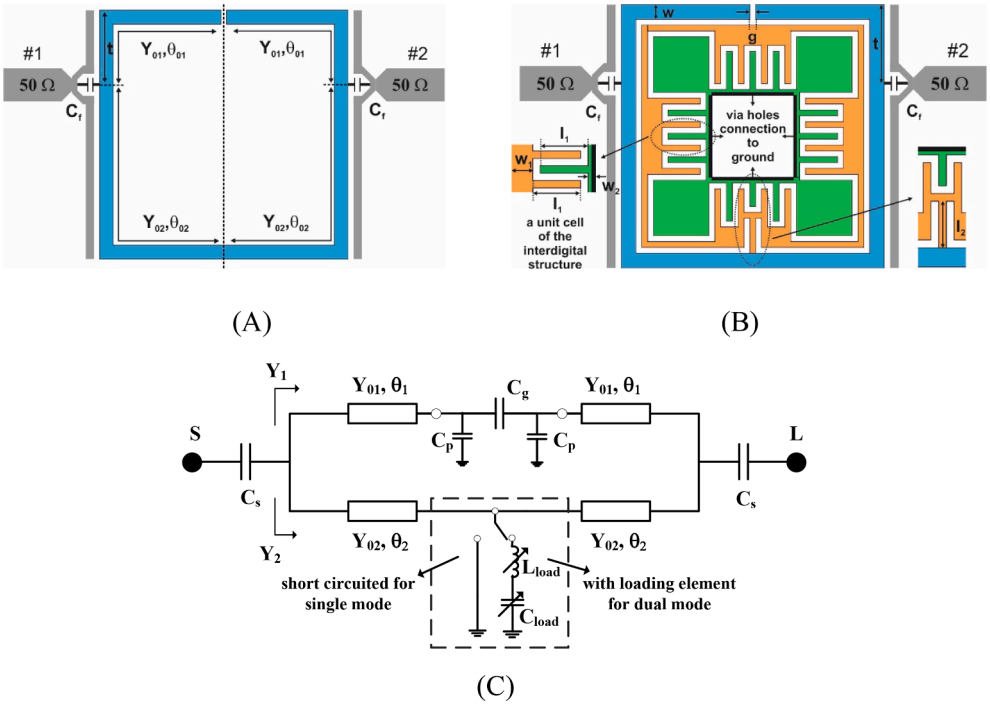

Fig. 7. The configuration of (A) single-mode (B) dual-mode resonator and (C) the equivalent circuit of the open loop resonator with/without a loading element.

equivalent circuit having the loading element is divided into two equal parts along the symmetry axis. The even/odd mode input admittances can be expressed as,

$$Y_{even/odd} = \left(\frac{1}{j\omega C_s} + \frac{1}{Y_1^{even/odd} + Y_2^{even/odd}}\right)^{-1} \tag{23}$$

where C_s represents the coupling between I/O ports and the resonator. $Y_1^{even/odd}$ and $Y_2^{even/odd}$ are the input admittances seen from the top and bottom arms of the equivalent circuit under even/odd mode excitation. For even mode excitation, the input admittances seen from the top/bottom arms can be calculated as,

$$Y_1^{even} = jY_{01}\frac{b_{ge} + \tan(\theta_1)}{1 - b_{ge}\tan(\theta_1)} \tag{24}$$

$$Y_2^{even} = jY_{02}\frac{b_{le} + \tan(\theta_2)}{1 - b_{le}\tan(\theta_2)} \tag{25}$$

where b_{ge} and b_{le} are susceptances of the gap and the loading element for even mode excitation, which can easily be found by using;

$$b_{ge} = \omega C_p Z_{01} \tag{26}$$

$$b_{le} = \left(\omega L_{load} - \frac{1}{\omega C_{load}}\right)^{-1}\frac{Z_{01}}{2}. \tag{27}$$

Even mode resonance condition is determined by equating the imaginary parts of Y_{even} to zero. Hence, the even mode resonance condition can be written as,

$$b_{ge} + b_{le} + (1 - b_{ge}b_{le})\tan(\theta_1 + \theta_2) = 0 \tag{28}$$

For odd mode excitation, the input admittances seen from the top and bottom arms can be calculated as,

$$Y_1^{odd} = jY_{01}\frac{b_{go} + \tan(\theta_1)}{1 - b_{go}\tan(\theta_1)} \tag{29}$$

$$Y_2^{odd} = -jY_{02}\cot(\theta_2) \tag{30}$$

where b_{go} is susceptance of the equivalent circuit of the gap for odd mode excitation and determined by

$$b_{go} = \omega(C_p + 2C_g)Z_{01}. \tag{31}$$

Similarly, the odd mode resonance condition can be found by equating imaginary part of input admittances (Y_{odd}) of the circuit to zero under odd mode excitation

$$b_{go}\tan(\theta_1 + \theta_2) - 1 = 0 \tag{32}$$

It should be noted from (28) and (32) that the odd mode resonance condition does not include any parameters related to the loading element, while the even mode resonance condition is calculated based on the parameters of the loading element. The center frequency of the proposed resonator can be calculated by the arithmetic mean of the even and odd mode resonance frequencies [21]. Hence, the center frequency and bandwidth are controlled depending on the gap, tap point position of the resonator, and dimensions related to the loading element, respectively. Finally, the dimensions of the resonators can be determined by employing the formula sets (23)-(32) in order to obtain the desired center frequency.

The circumference of the resonator is an important factor in determining the fundamental resonant frequency, and the mode due to the resonator size is called odd mode. When the gap of the open loop resonator (g) increases, the perimeter of the open loop resonator decreases, and the odd mode frequency (f_{odd}) and coupling coefficient (k) change, as can be seen in Fig. 8(A). Another parameter related to determining the odd mode frequency is the tap point position (t) of the feed lines. Variation of the tap point affects the frequency response and coupling coefficient, as illustrated in Fig. 8(B). In these figures, the solid and dashed lines represent the status of the capacitively loaded open loop resonator having transmission zeros on the left and right side of the passband, respectively.

The loading element is constructed by interdigital unit cells which increase the capacitance per unit length, and hence the propagation velocity decreases and the even mode resonance frequency shifts down. Effects of the lengths of the capacitive fingers and the inductive line on the even mode frequency characteristics (f_{even}) and coupling coefficient

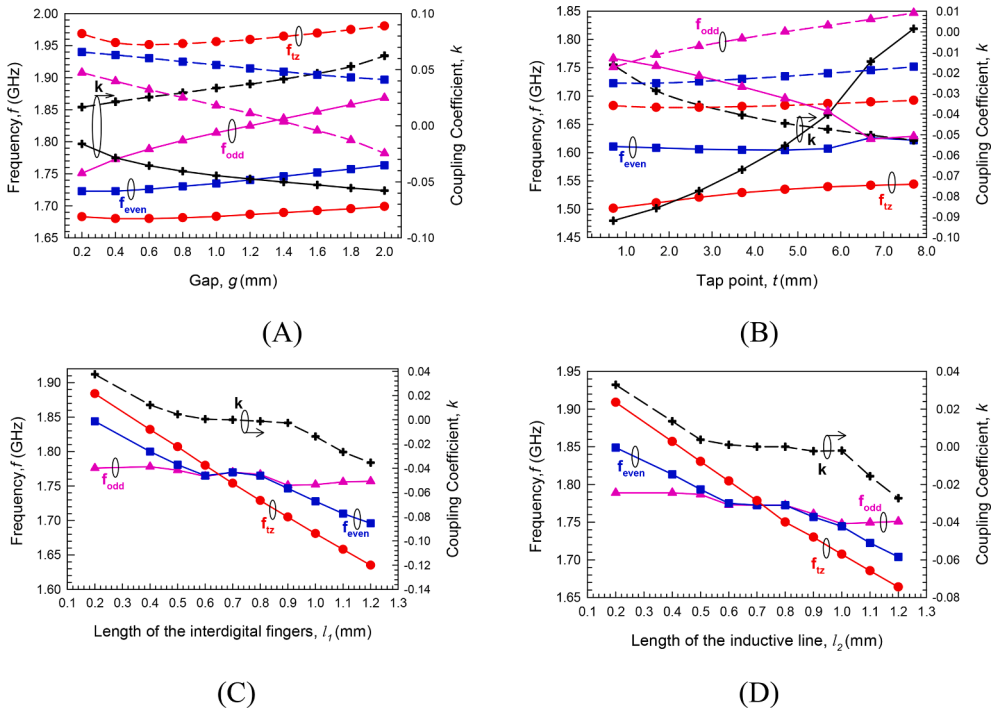

Fig. 8. The frequency response and coupling coefficient of the capacitively loaded open loop resonator: for different values of (A) g, (B) t, (C) l_1 and (D) l_2 (for C_p = 2.0 pF).

Table 3
Dimensions of the capacitively loaded open loop resonator for Fig. 8.

		g (mm)	*t (mm)*	*l_1 (mm)*	*l_2 (mm)*
(a)	solid lines	variable	1.7	0.3	0.4
	dashed lines	variable	1.7	0.8	1.0
(b)	solid lines	0.2	variable	0.4	0.8
	dashed lines	0.2	variable	1.4	1.2
(c)		0.2	1.7	variable	0.8
(d)		0.2	1.7	0.7	variable

(k) are shown in Fig. 8(C) and Fig. 8(D), respectively. As can be seen from the figures, the even mode resonance frequency and the location of the transmission zero can be controlled by using the lengths of the interdigital fingers and the inductive line (l_1, l_2), which are the most effective parameter of the proposed design so that the transmission zero can easily be moved on a wide frequency range and located on the desired side of the passband. All dimensions of the capacitively loaded open loop resonator to obtain simulated responses illustrated in Fig. 8 are given in Table 3.

In order to move transmission zero to provide higher selectivity in the desired edge of the passband, the dimensions of the loading elements should be adjusted to suitable values while the total surface area of each open loop resonator is fixed, or vice versa. The even mode frequency can be lower/higher than that of the odd mode by increasing/decreasing the length of the interdigital fingers (l_1) and inductive line (l_2) so that the transmission zero is expected to shift from the right (left) side to the left (right) side of the passband. An interdigital loaded resonator excites dual-mode in a narrow passband. A narrow passband is significant for high selectivity and external quality factor (Q_e). To exhibit the difference between the quality factors of single and dual-mode open loop resonators, insertion losses of half wavelength microstrip open loop resonator and proposed dual-mode open loop resonator are compared in normalized frequency, as illustrated in Fig. 9(A). The figure shows normalized frequency responses of the single-mode resonator and dual-mode open loop resonator having a transmission zero on the left (DMR#1) and right (DMR#2) side of the passband. It is necessary to determine the bandwidth to calculate the external quality factor based on the fractional bandwidth. As illustrated in Fig. 9(A), the loaded open loop resonator

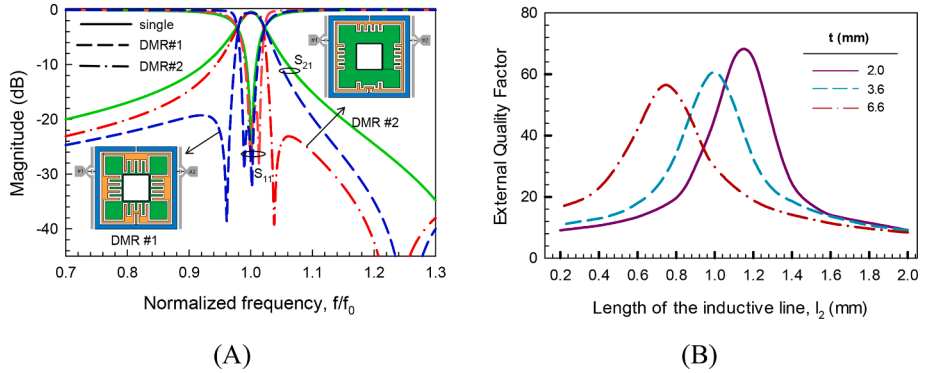

Fig. 9. (A)The comparison of S parameters for the single-mode and dual-mode open loop resonators (B) the effect of l_2 on external quality factor versus different tap point position for dual-mode. (w = 0.5, g = 0.2, l_1 = 0.7, w_1 = 1.3, w_2 = 0.2, all units in mm and C_f = 0.2 pF.).

having transmission zero on the left or right side of the passband has a narrower bandwidth than that of a single-mode resonator. Therefore, the quality factor of the microstrip open loop resonator with a loading element is higher than that of the single-mode resonator. It can be seen in Fig. 9(A) that the transmission zero can be located on each side of the passband by controlling parameters related to the loading element.

It is well known that the tap point position is a significant and necessary parameter for calculating the external quality factor (Q_e). Although the tap point position does not change the transmission zero and even mode frequency, it affects the quality factor since it changes the odd mode frequency, as described above. For these reasons, the effect of the length of the inductive line (l_2) on the external quality factor is also investigated for different tap point positions in the dual-mode resonator. Fig. 9(B) depicts the behavior of the external quality factor for the capacitively loaded resonator having a transmission zero on the right side of the passband depending on three different tap point locations. It can be seen that the external quality factor also increases when the length of l_2 is increased. As a result of the above discussion, it is clear that flexible control of the frequency response is available.

Each capacitively loaded open loop resonator can generate two modes and one transmission zero. The design of multi-mode BPFs is based on a dual-mode property with a proper coupling strength between I/O ports. Two dual-mode resonators should be coupled to each other to increase the number of transmission poles and zeros. The type of coupling also changes depending on the orientation of the open loop resonators. The loading element adds one more transmission pole within each passband and one transmission zero near the stopbands. Distance between the resonators affects the bandwidth and locations of the transmission poles within each passband. Based on the proposed method, a multi-mode bandpass filter with a higher selectivity can be designed by coupling two loaded resonators having different electrical lengths, as known from [22,23].

The next stage is to design the dual and quad-mode diplexer by applying the flowchart in Fig. 6(B).

3.2. Dual-mode diplexer application

Two second-order bandpass filters with different sizes are designed to form the lower and higher passband of the diplexer. The proposed diplexer is constructed by the two bandpass filters (BPF#1 and BPF#2) and a *T*-junction as illustrated in Fig. 10(A). Fig. 10(B) shows 3D image of the diplexer. For the design, firstly, the resonator dimensions were determined according to the desired center frequency, and a loading element was used to obtain a dual mode. Loading element parameters are determined according to the desired second mode frequency and the position of the transmission zero. It has been determined that the dimensions could be as follows. BPF#1 and BPF#2 have a loading element consisting of interdigital fingers of 0.2 and 0.7 mm in length, respectively. The spacing between the interdigital fingers is taken as 0.2 mm in both filter circuits. The interdigital loading elements are connected to the resonator by an inductive line with length of 0.2 mm (for BPF#1) and 0.4 mm (for BPF#2). The gap of both open loop resonators is 0.2 mm, and the tap point position of the feed lines is adjusted to be 3.0/2.0 mm in BPF#1/BPF#2. I/O ports are fed by a lumped capacitor to achieve the required coupling strength in both passbands. The lumped capacitors (C_f) are used to increase coupling levels due to the high energy loss in the interdigital cells. Their capacitance values are taken as 0.2 and 0.1 pF in BPF#1 and BPF#2, respectively. Values of the capacitor have been determined based on the even–odd mode analysis. The capacitance of the lumped capacitors should be adjusted to a convenient value that the bandwidth and return loss to be the desired level in the passband. The total surface area of the proposed circuit is 26.8 mm × 11.5 mm. The layout of the filters given in Fig. 10(B) is optimized through a full wave EM simulator [24]. The simulated response of the proposed diplexer is illustrated in Fig. 10(C). To obtain the required impedance matching, the input impedance at the *T*-junction is determined by the conditions specified in [25]. These conditions can be ensured by using the *T*-shaped microstrip line, which provides an open circuit at the frequency of the other passband. As can be seen from Fig. 10(D), the input impedances of BPF#1 at 2.12 GHz and BPF#2 at 1.75 GHz are very low and so close to the shorted circuit as depicted in

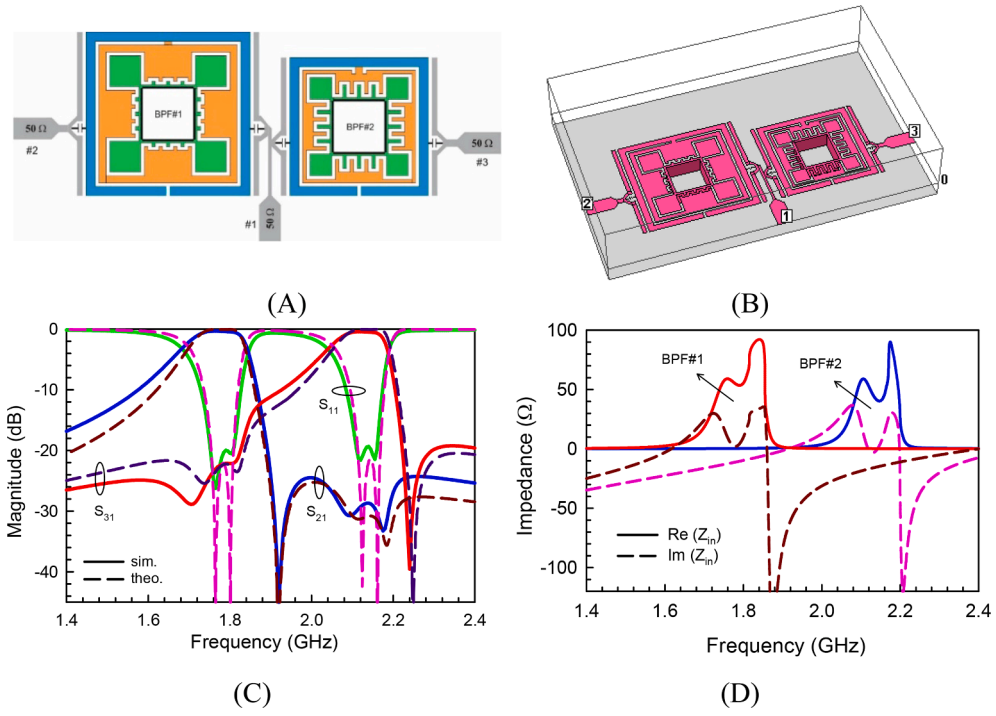

Fig. 10. (A) Configuration, (B) 3D image, (C) the comparison of the simulated and calculated frequency response of the dual-mode diplexer, (D) input impedances of the BPF#1 and BPF#2.

Table 4
The coefficients of characteristic polynomial for the dual-mode diplexer.

Coefficients (c_n)	Rational Characteristic Polynomials $\sum_{n=0}^{4} c_n s^n = c_4 s^4 + c_3 s^3 + c_2 s^2 + c_1 s^1 + c_0$			
	$E(s)$	$F(s)$	$P_r(s)$	$P_t(s)$
c_4	1	1	–	–
c_3	2.315 – 1.879i	−1.879i	0.521	−0.391
c_2	11.580 – 3.606i	9.113	0.291 – 0.236i	−0.234 + 2.078i
c_1	11.987 – 11.966i	−0.326 – 9.196i	6.326 – 0725i	2.397 + 0.658i
c_0	24.719 – 2 626i	23.873 + 0.231i	1.975 + 6.601i	−0.160 + 0.650i

[25]. Two transmission lines with high impedances are needed for transforming these low impedances into an open circuit at the junction. Finally, the lengths of the *T*-junction and tap point distance of the channel filters are optimized such that each filter in the diplexer has the best return and insertion loss level in the passband and a good isolation level between channels.

To demonstrate the use of the proposed theoretical approach in practical diplexer applications, the characteristic polynomials for the dual-mode diplexer constructed with the open-loop resonators by sequentially applying the synthesis procedure steps described in Section 2 are found as given in Table 4.

The characteristic polynomials are used to determine the coupling matrix of the proposed diplexer. The input port of each channel is directly connected to the common port of the diplexer, as shown in Fig. 10(B). A transversal coupling diagram in Fig. 2(A) can be used for this configuration of dual-mode diplexer. In this case, it can be defined (7 × 7) coupling matrix for this three-port circuit having dual-mode channel filters, as can be seen in (33). The values of the coupling elements available according to the coupling diagram are computed as given in this coupling matrix. The simulated and calculated frequency response are compared in Fig. 10(C).

$$\begin{bmatrix} & \mathbf{S} & \mathbf{1} & \mathbf{2} & \mathbf{L_1} & \mathbf{3} & \mathbf{4} & \mathbf{L_2} \\ \mathbf{S} & 0 & 0.627 & 0.407 & 0 & 0.644 & 0.429 & 0 \\ \mathbf{1} & 0.627 & -2.452 & 0 & -0.601 & 0 & 0 & 0 \\ \mathbf{2} & 0.407 & 0 & -1.302 & 0.466 & 0 & 0 & 0 \\ \mathbf{L_1} & 0 & -0.601 & 0.446 & 0 & 0 & 0 & 0 \\ \mathbf{3} & 0.644 & 0 & 0 & 0 & 2.247 & 0 & 0.668 \\ \mathbf{4} & 0.429 & 0 & 0 & 0 & 0 & 3.386 & -0.395 \\ \mathbf{L_2} & 0 & 0 & 0 & 0 & 0.668 & -0.395 & 0 \end{bmatrix} \tag{33}$$

3.3. Quad-mode diplexer application

The high selective microstrip diplexer is performed by fourth-order dual-mode microstrip filters having two different sizes. Transmission zeros of a channel filter have been arranged at the other channel filter passband to improve the diplexer isolation in this design. The fourth-order microstrip filter is designed by using the two coupled microstrip open loop resonators with the properties detailed in Section 3.1. The dual-mode resonators used in the design have a narrow band frequency response with a transmission zero and, two modes so the proposed filter has high selectivity and quality factor. High selectivity is achieved by locating three finite transmission zeros in each channel filter design. To obtain the proposed high selective channel filter the single-mode two identical microstrip open loop resonators are situated with an appropriate gap and investigated with an EM simulator, firstly [24]. In this case, two degenerate modes appear and a transmission zero occurs on the right side of the passband which is inherent with the structure and so-called natural TZ. These modes are the odd modes and resulted from the coupling of the identical single-mode resonators. A natural transmission zero can be located on the desired side of the passband, depending on the different orientations of a pair of open loop resonators. It is obvious that any coupling type in those structures is basically related to fringe fields. The configuration is arranged for the mixed-coupling type. Similarly, when two identical open loop resonators with loading elements have coupled to each other, the four poles and three transmission zeros are excited, as estimated. A transmission zero

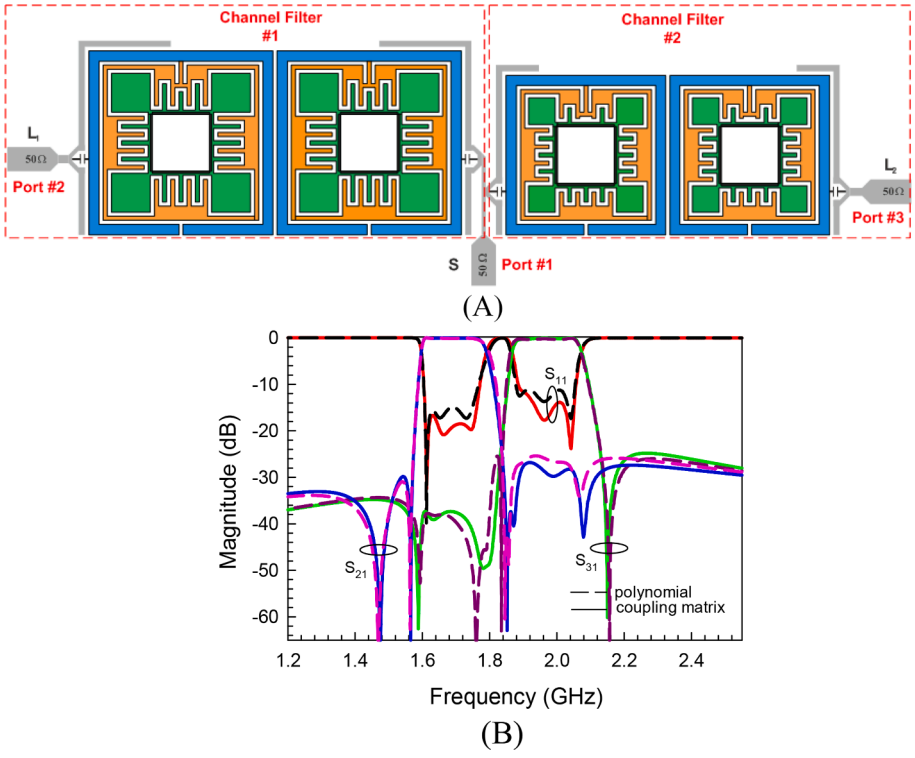

Fig. 11. (A) Configuration of the quad mode diplexer (B) comparison of the calculated polynomial and coupling matrix response.

Table 5
Dimensions of the quad mode diplexer.

Channel Filters	Parameters (mm)						
	w	g	t	l_1	l_2	w_1	w_2
#1	0.5	0.2	3.0	1.3	1.1	0.7	0.2
#2	0.5	0.2	1.4	0.7	1.3	0.7	0.2

on the right side of the passband is a natural transmission zero occurred depending on the tap position of I/O ports and the orientation of the resonators. The others arise from the configuration of the loading element. Thus, the position of the first transmission zero (at the right side of the passband) does not change, while the other two zeros can be moved to the desired stopbands by adjusting the parameters of the loading element.

The high selective microstrip diplexer shown in Fig. 11(A) is achieved by fourth-order filters having two resonators of different sizes. Two dual-mode resonators are combined by a *T*-shaped open ended input feed line to obtain the proposed diplexer. To obtain the required impedance matching, the input impedances of the diplexer at the *T*-junction are adjusted to be 50 Ω at the center frequency of the related channel filters. There is no need for any impedance matching circuit with the proposed configuration, which is result in reduced circuit size. The total surface area of the proposed circuit is 44.2 mm × 12.0 mm. To verify the above theoretical analysis and optimize the proposed BPFs with a reduced-size and a high selectivity, a full-wave EM simulation is carried out by using a full wave EM Simulator [24]. The optimized dimensions of the channel filters used in the diplexer design are represented in Table 5. The transmission zero of each resonator needs to be carefully located to achieve high isolation between two channels in the design of the diplexer. As can be seen in Fig. 11(B), the diplexers have two transmission zeros on the left side and one transmission zero on the right side of the passband for each filter channel. Two transmission zeros are located on the left side of the passband since the even mode frequency is lower than that of the odd mode. It means that the transmission zeros can be moved to the right side of the passband by increasing the electrical length of the loading element. The natural transmission zero located on the right side of the passband is resulted from different orientations of a couple of dual-mode open loop resonators, which are coupled by proper spacing. As a result of the transmission zeros on both sides of the passband, the proposed diplexer by using multi-mode resonators has high selectivity.

Similarly, the characteristic polynomials of the proposed quad-mode diplexer can be achieved according to the procedure steps in Section 2. The characteristic polynomial coefficients of the quad-mode diplexer are given in descending order, as can be seen in Table 6. Since quad-mode channel filters are used in the design, an (11 × 11) coupling matrix is obtained by means of the calculated characteristic polynomials. The values of the coupling matrix elements are shown in (34). The comparison of the frequency response computed using the polynomial synthesis procedure and the coupling matrix synthesis method is illustrated in Fig. 11(B).

$$
\begin{bmatrix}
 & \mathbf{S} & \mathbf{1} & \mathbf{2} & \mathbf{3} & \mathbf{4} & \mathbf{L_1} & \mathbf{5} & \mathbf{6} & \mathbf{7} & \mathbf{8} & \mathbf{L_2} \\
\mathbf{S} & 0 & 0.698 & 0.602 & 0.285 & 0.516 & 0 & 0.508 & 0.662 & 0.475 & 0.143 & 0 \\
\mathbf{1} & 0.698 & -1.320 & 0 & 0 & 0 & -0.662 & 0 & 0 & 0 & 0 & 0 \\
\mathbf{2} & 0.602 & 0 & -2.758 & 0 & 0 & 0.622 & 0 & 0 & 0 & 0 & 0 \\
\mathbf{3} & 0285 & 0 & 0 & -0.417 & 0 & 0.412 & 0 & 0 & 0 & 0 & 0 \\
\mathbf{4} & 0.516 & 0 & 0 & 0 & -3.049 & -0.259 & 0 & 0 & 0 & 0 & 0 \\
\mathbf{L_1} & 0 & -0.662 & 0.622 & 0.412 & -0.259 & 0 & 0 & 0 & 0 & 0 & 0 \\
\mathbf{5} & 0.508 & 0 & 0 & 0 & 0 & 0 & 2.385 & 0 & 0 & 0 & -0.301 \\
\mathbf{6} & 0.662 & 0 & 0 & 0 & 0 & 0 & 0 & 1.729 & 0 & 0 & 0.598 \\
\mathbf{7} & 0.475 & 0 & 0 & 0 & 0 & 0 & 0 & 0 & 0.588 & 0 & -0.417 \\
\mathbf{8} & 0.143 & 0 & 0 & 0 & 0 & 0 & 0 & 0 & 0 & 0.261 & 0.292 \\
\mathbf{L_2} & 0 & 0 & 0 & 0 & 0 & 0 & -0.301 & 0.598 & -0.417 & 0.292 & 0
\end{bmatrix} \tag{34}
$$

Table 6
The coefficients of the rational characteristic polynomials for quad mode diplexer.

Coefficients (c_n)	Rational Characteristic Polynomials $\sum_{n=0}^{8} c_n s^n = c_8 s^8 + c_7 s^7 + c_6 s^6 + c_5 s^5 + c_4 s^4 + c_3 s^3 + c_2 s^2 + c_1 s^1 + c_0$			
	$E(s)$	$F(s)$	$P_r(s)$	$P_t(s)$
c_8	1	1	–	–
c_7	−4.281 + 2.581i	2.581i	0.240	−0.179
c_6	15.181 – 9.104i	6.063	−0.218 + 0.798i	0.221 – 0.878i
c_5	−34.958 + 29.784i	2.371 + 14.696i	3.659 – 0.996i	−0.292 + 0.707i
c_4	58.765 – 53.072i	8.640 + 3.876i	−1.958 + 5.066i	1.374 – 7.242i
c_3	−70.380 + 65.275i	11.465 + 17.569i	19.635 – 6.391i	12.062 + 6.325i
c_2	48.709 – 37.186i	2.316 + 9.940i	−9.600 – 13.204i	−5.708 + 6.875i
c_1	−18.626 + 9.352i	7.788 + 6.369i	−3.087 + 3.196i	−1.031 – 1.322i
c_0	2.921 – 0.451i	2.923 + 0.198i	0.295 + 0.233i	−0.080 + 0.069i

4. Experimental applications

Based on the above analysis, the proposed dual-mode and quad-mode circuits are designed. To demonstrate the proposed approaches, the two designed circuits have been fabricated on RT/Duroid substrate with a relative dielectric constant of 10.2 and a thickness of 1.27 mm as shown in Fig. 12. The characteristic impedance of microstrip feed lines is 50 Ω and the fabricated circuits are fed by 50 Ω connectors. The measurements are realized by Agilent E5071C Network Analyzer. The first circuit is a dual-mode diplexer circuit as shown in Fig. 12(A). The overall size of the circuit is 26.8 mm × 11.5 mm. The center frequencies of the channel filters are measured as 1.76 GHz and 2.12 GHz. The insertion loss changes between the −1.6 dB and −2.2 dB for the first passband while it changes between the −1.2 dB and −1.9 dB for the second passband, as illustrated in Fig. 12(A). The fabricated quad-mode diplexer circuit has a surface area of 44.2 mm × 12 mm as shown in Fig. 12(B). All four transmission poles and four transmission zeros appear in the measured frequency response. It is clear from Fig. 12(B) that a natural transmission zero occurs between the two passbands. Due to the presence of transmission zeros on both sides of passbands of channel filters, the proposed diplexer has considerable selectivity. The measured center frequencies of the two channels are 1.66 GHz and 1.95

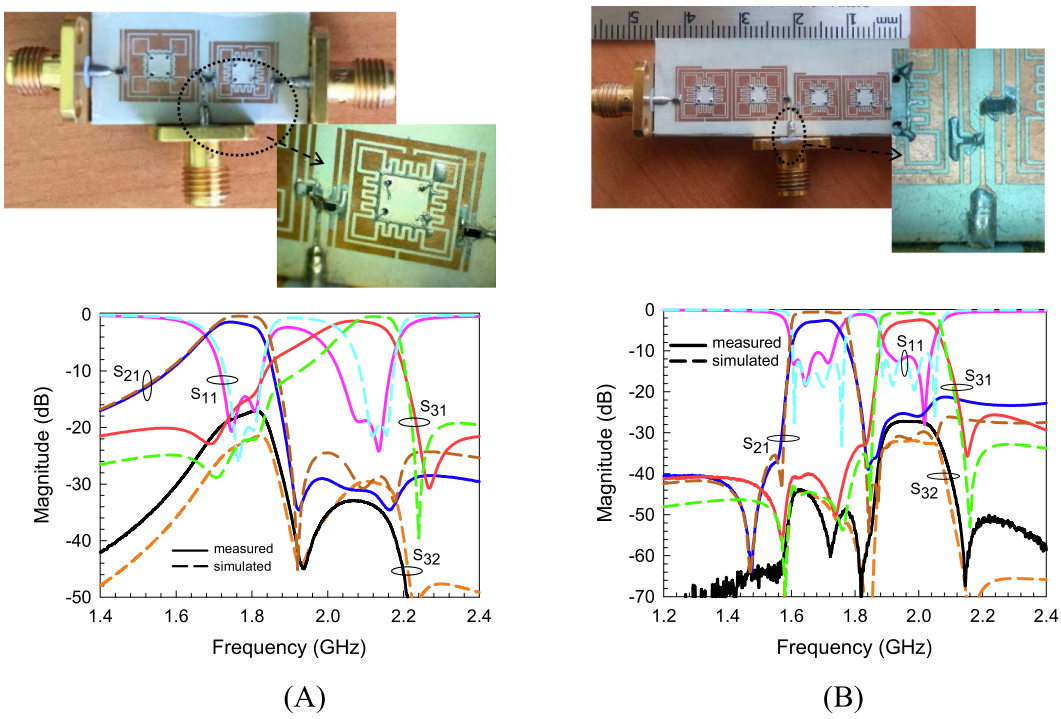

Fig. 12. Fabricated photographs and comparison of the simulated and measured frequency response of the proposed diplexers (A) dual-mode (B) quad-mode diplexer.

Table 7
Comparison between dual/quad mode diplexers.

Refs.	f_{01} / f_{02} (GHz)	Order	3-dB FBW (%)	IL (dB)	Band isolation (dB)			Size (λ_g^2)
					First	Second	Out of	
[26]	2.41 / 3.61	2	6.7 / 3.6	1.46 / 2.15	>38	>38	>50	0.099
[27]	2.44 / 3.52	2	–	1.43 / 1.59	>45	>42	>45	0.283
[28]	1.1 / 1.3	2	8.0 / 9.2	1.83 / 1.52	>40	>30	>60	0.705
This work	**1.76 / 2.12**	**2**	**9.1 / 9.6**	**1.4 / 1.6**	**>20**	**>30**	**>50**	**0.073**
[29]	2.13 / 2.65	3	8.6 / 9.3	1.9 / 1.6	–	–	–	0.310
[30]	1.0 / 1.2	4	10.0 / 9.0	2.24 / 2.22	>40	>40	>27	0.22
[31]	1.75 / 1.95	4	4.0 / 4.0	2.88 / 2.95	>50	>50	>50	0.391
[32]	2.4/ 2.8	4	9.1 / 10.7	2.13 / 1.95	>32	>40	>45	0.127
This work	**1.66 / 1.95**	**4**	**11.5 / 10.1**	**2.9 / 2.8**	**>45**	**>30**	**>55**	**0.111**

*λ_g is the guided wavelength at the center frequency of the passband.

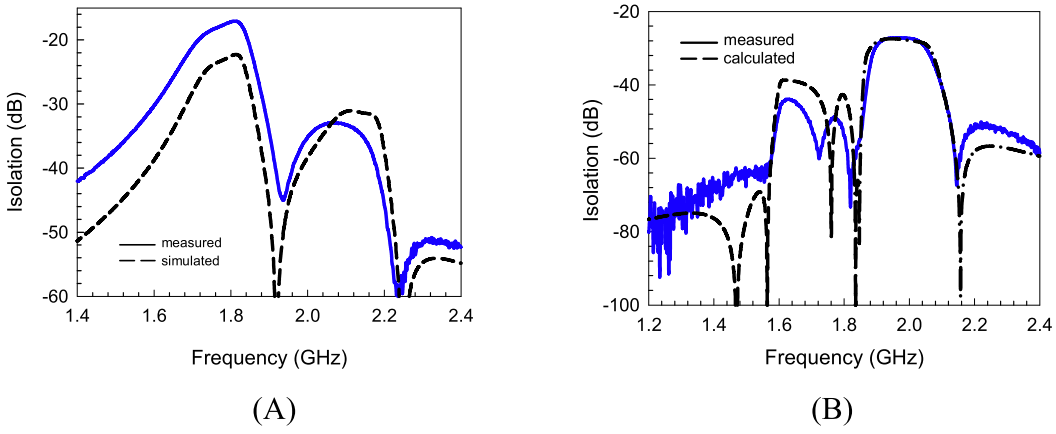

Fig. 13. Comparison of the measured and calculated isolation of the proposed diplexers; (A) dual-mode, (B) quad-mode diplexer.

GHz with insertion losses of approximately −2.9 dB and −2.8 dB, respectively. Out of the band rejection for each channel is measured below −20 dB. Table 7 exhibits the comparison among the proposed dual/quad mode diplexer and some studies in the literature. It can be seen from Table 7 that the proposed diplexers have compact sizes, close channel bands and sufficient isolation. The isolation for out-of-band is obtained as better than the 50 dB level aimed design value, this isolation level is better than some studies in the literature as shown in Table 7. Also, the comparison of the measured and calculated isolation level of the dual/quad mode diplexer is depicted in Fig. 13.

When the photographs of the produced diplexers given in Fig. 12 are viewed in detail, it can be seen that there are some production difficulties such as the connection of the interdigital parallel capacitor to the ground and the lumped serial capacitors to the feed lines. Unfortunately, these difficulties result in a negative effect on the measurement results because of production in our individual laboratory. The effect of the conductor and dielectric loss on the frequency responses must be considered in the proposed design process. Especially, the effect on the measured results is a little more than that of simulation as can be seen from the differences between the measurement and simulated results in the bandwidth. This effect can be considered a disadvantage for designers. However, this disadvantage can be annihilated by decreasing the manufacturing tolerances and measurement difficulties.

5. Conclusion

A design procedure for microstrip multi-mode diplexer realized with high selectivity and compact size has been presented in this paper. A theoretical approach is discussed to indicate the design procedure for the diplexer having close TX and RX bands. The theoretical approach for the proposed diplexers has been described by using a polynomial synthesis procedure and the coupling matrix synthesis method. The proposed diplexers are designed using open loop resonators and interdigital loading elements that allow easy determination of the center frequencies of each channel filter. Two configurations, including two types of diplexers a dual-mode and a quad-mode, have been designed and performed to verify the theoretical approach and to demonstrate practical design. The efficiency of the interdigital unit cells and the placement of the loading element inside the resonator have been resulted in a more compact structure property. Having sufficient power distribution for each channel filter with a simple feed line configuration and not using an extra matching circuit are important advantages. Taking advantage of the multi-mode generated by the capacitively-loaded open loop resonators, the lower and higher channel filters achieve high selectivity. Moreover, controllable transmission zeros have been created by these compact structures to improve the selectivity of both passbands with an acceptable isolation level. Finally, the designed circuits were simulated and fabricated to illustrate their validity. The measurements were obtained in good agreement with the predicted and simulated results.

Declaration of Competing Interest

The authors declare that they have no known competing financial interests or personal relationships that could have appeared to influence the work reported in this paper.

Acknowledgment

This work has been supported the Scientific and Technological Research Council of Türkiye (TUBITAK) under Grant 120E101.

References

[1] Roshani S, Roshani S. Design of a very compact and sharp bandpass diplexer with bended lines for GSM and LTE applications. AEU-Int J Electron C 2019;99:354–60.
[2] Gorur AK, Ozturk Ozdemir P, Sahin GE, Karpuz C. A novel microstrip diplexer design with tunable bandwidths and switchable channels for 4.5G applications. Turk J Electr Eng Comput Sci 2017;25:4445–56.
[3] Wong S, Zheng B, Lin J, Zhang Z, Yang Y, Zhu L, et al. Design of three-state diplexer using a planar triple-mode resonator. IEEE Trans Microw Theory Tech Sept. 2018; 66(9):4040–6.
[4] Gomez Garcia R, Munoz-Ferreras J, Psychogiou D. Quasi-elliptic-type multiplexer design without cross coupling. IEEE Microwave Wirel Compon Lett Sept. 2018;28 (9):801–3.
[5] Zhang Z, Wong S, Lin J, Liu H, Zhu L, He Y. Design of multistate diplexers on uniform- and stepped-impedance stub-loaded resonators. IEEE Trans Microw Theory Tech April 2019;67(4):1452–60.
[6] Yahya SI, Rezaei A, Nouri L. Compact wide stopband microstrip diplexer with flat channels for WiMAX and wireless applications. IET Circuits, Dev Syst 2020;14(6): 846–52.
[7] Upadhyaya T, Pabari J, Sheel V, Desai A, Patel R, Jitarwal S. Compact and high isolation microstrip diplexer for future radio science planetary applications. AEU - Int J Electron Commun 2020;127:153497.
[8] Rezaei A, Yahya SI, Jamaluddin MH. A novel microstrip diplexer with compact size and high isolation for GSM applications. AEU - Int J Electron Commun Feb 2020: 114.
[9] Liu H, Xu W, Zhang Z, Guan X. Compact diplexer using slotline stepped impedance resonator. IEEE Microwave Wirel Compon Lett Feb. 2013;23(2):75–7.
[10] Guan X, Yang F, Liu H, Zhu L. Compact and high-isolation diplexer using dual-mode stub-loaded resonators. IEEE Microwave Wirel Compon Lett June 2014;24 (6):385–7.
[11] Chuang M, Wu M. Microstrip Diplexer Design Using Common T-Shaped Resonator. IEEE Microwave Wirel Compon Lett Nov. 2011;21(11):583–5.
[12] Zhu C, Yao L, Zhou J. Novel microstrip diplexer based on a dual-band bandpass filter for WLAN system. Asia-Pacific Microwave Conference 2010:1102–5.
[13] Deng P, Wang C, Chen CH. Compact microstrip diplexers based on a dual-passband filter. Asia-Pacific Microwave Conference 2006:1228–32.
[14] Macchiarella G, Tamiazzo S. Novel approach to the synthesis of microwave diplexers. IEEE Trans Microw Theory Tech Dec. 2006;54(12):4281–90.
[15] Garcia-Lamperez A, Salazar-Palma M, Sarkar TK. Analytical synthesis of microwave multiport networks. IEEE MTT-S Int Microwave Sympos Digest 2004: 455–8.
[16] Gorur A. Description of coupling between degenerate modes of a dual-mode microstrip loop resonator using a novel perturbation arrangement and its dual-mode bandpass filter applications. IEEE Trans Microw Theory Tech Feb. 2004;52 (2):671–7.
[17] Hong J, Shaman H, Chun Y. Dual-mode microstrip open-loop resonators and filters. IEEE Trans Microw Theory Tech Aug. 2007;55(8):1764–70.
[18] Hong JS, Lancaster MJ. Microstrip filters for RF/microwave applications. New York: Wiley; 2001.
[19] Cameron RJ. General coupling matrix synthesis methods for Chebyshev filtering functions. IEEE Trans Microw Theory Tech April 1999;47(4):433–42.
[20] Cameron RJ. Advanced coupling matrix synthesis techniques for microwave filters. IEEE Trans Microw Theory Tech Jan. 2003;51(1):1–10.
[21] Lei MF, Wang H. An analysis of miniaturized dual-mode bandpass filter structure using shunt-capacitance perturbation. IEEE Trans Microw Theory Tech March 2005;53(3):861–7.
[22] Karpuz C, Ozdemir PO, Firat GB. Design of fourth order dual-mode microstrip filter by using interdigital capacitive loading element with high selectivity. *46th European Microwave Conference (EuMC)*, London, England, 2016:461-464.
[23] Karpuz C, Ozdemir PO. Design of fourth order microstrip filter using the open loop resonator with a novel interdigital loading element. *IEEE MTT-S International Microwave Symposium (IMS)*, Honolulu, HI, USA, 2017:1819-1822.
[24] EM User's Manual, *Sonnet Software*, Inc, Liverpool, NY; 2008.
[25] Yang T, Chi PL, Itoh T. High isolation and compact diplexer using the hybrid resonators. IEEE Microwave Wirel Compon Lett Oct. 2010;20(10):551–3.
[26] Xiao J, Zhang M, Ma J. A compact and high-isolated multiresonator-coupled diplexer. IEEE Microwave Wirel Compon Lett Nov. 2018;28(11):999–1001.
[27] Xiao J, Zhu M, Li Y, Tian L, Ma J. High selective microstrip bandpass filter and diplexer with mixed electromagnetic coupling. IEEE Microwave Wirel Compon Lett Dec. 2015;25(12):781–3.
[28] Chen D, Zhu L, Bu H, Cheng C. A novel planar diplexer using slotline-loaded microstrip ring resonator. IEEE Microwave Wirel Compon Lett Nov. 2015;25(11): 706–8.
[29] Guo J, Wong S, Xie Z, Zhang L, Zhu L, He Y. A Compact Planar Diplexer Using Common Dual-Mode Rectangular Patch Resonators. *International Conference on Microwave and Millimeter Wave Technology (ICMMT)*, Guangzhou, China, 2019:1-3.
[30] Chen F, Hu HT, Li RS, Chen JF, Luo D, Chu QX, et al. Design of Wide-Stopband Bandpass Filter and Diplexer Using Uniform Impedance Resonators. IEEE Trans Microw Theory Tech Dec 2016;64:4192–203.
[31] Nwajana AO, Yeo KSK. Multi-coupled resonator microwave diplexer with high isolation. *46th European Microwave Conference (EuMC)*, London, UK, 2016:1167-1170.
[32] Shao Q, Chen FC. Design of compact diplexer with novel matching network using cascaded quadruplet filters. Microwave Opt Technol Lett Feb 2017;59(2):315–8.